nanomaterials

MDPI

Article

Pure Acetylene Semihydrogenation over Ni–Cu Bimetallic Catalysts: Effect of the Cu/Ni Ratio on Catalytic Performance

Shuzhen Zhou [1,2], Lihua Kang [1,2], Xuening Zhou [2], Zhu Xu [2] and Mingyuan Zhu [1,*]

[1] College of Chemistry and Chemical Engineering, Yantai University, Yantai 264004, China; Shuzhenzhou@163.com (S.Z.); lhkang@ytu.edu.cn (L.K.)

[2] School of Chemistry and Chemical Engineering, Shihezi University, Shihezi 832003, China; zhouxuening@stu.shzu.edu.cn (X.Z.); xz20200217@126.com (Z.X.)

* Correspondence: zhuminyuan@shzu.edu.cn; Tel.: +86-993-205-7270

Received: 14 February 2020; Accepted: 7 March 2020; Published: 11 March 2020

Abstract: Ethylene is an important chemical raw material and with the increasing consumption of petroleum resources, the production of ethylene through the calcium carbide acetylene route has important research significance. In this work, a series of bimetallic catalysts with different Cu/Ni molar ratios are prepared by co-impregnation method for the hydrogenation of calcium carbide acetylene to ethylene. The introduction of an appropriate amount of Cu effectively inhibits not only the formation of ethane and green oil, thus increasing the selectivity of ethylene, but also the formation of carbon deposits, which improves the stability of the catalyst. The ethylene selectivity of the Ni–Cu bimetallic catalyst increases from 45% to 63% compared with the Ni monometallic counterpart and the acetylene conversion still can reach 100% at the optimal conditions of 250 °C, 8000 mL·g^{-1}·h^{-1} and V(H_2)/V(C_2H_2) = 3. X-ray diffraction and transmission electron microscopy confirmed that the metal particles were highly dispersed on the support, High-resolution transmission electron microscopy and H_2-Temperature programmed reduction proved that there was an interaction between Ni and Cu, combined with X-ray photoelectron spectroscopy and density functional theory calculations results, Cu transferred electrons to Ni changed the Ni electron cloud density in $NiCu_x$ catalysts, thus reducing the adsorption of acetylene and ethylene, which is favorable to ethylene selectivity.

Keywords: Ni–Cu; calcium carbide acetylene; selective hydrogenation; ethylene

1. Introduction

As an important petrochemical raw material, ethylene is currently produced by cracking hydrocarbon from petroleum feedstock such as naphtha and ethane [1,2]. With the increasing consumption of petroleum resources, the production of calcium carbide from coal, acetylene from calcium carbide and water, and then hydrogenation to ethylene has emerged as a new alternative approach to produce ethylene, which is more economically feasible in areas rich in coal resources.

Alkynes have stronger adsorbability than alkenes [3] and extensive research on the hydrogenation of acetylene in ethylene-rich streams has shown that the path of direct hydrogenation of acetylene to ethylene is fully feasible [4,5]. Scheme 1 summarizes a plausible reaction route for the acetylene hydrogenation. The adsorbed acetylene can react with the adsorbed hydrogen to form ethylene as the desired product, or hydro-oligomerize to form C_4H_6 hydrocarbons. Nondesorbed ethylene can be over-hydrogenated to form ethane [6,7]. In addition, ethylene selectivity also depends on the kinetics. Thus, for $k_2 >> k_4$, the desired ethylene products are obtained. For $k_1/k_{-1} >> k_3/k_{-3}$, the adsorption of acetylene may prevent the readsorption of ethylene, thereby preventing the rehydrogenation of ethylene [8]. Unfortunately, if $k_1/k_{-1} >> k_2/k_{-2}$, the adsorbed acetylene will hydro-oligomerize to

form C_4H_6, which is considered as the precursor of green oil and will lead to catalyst deactivation [9]. Therefore, in order to maximize the production of ethylene, ethylene overhydrogenation should be reduced and acetylene polymerization should be inhibited.

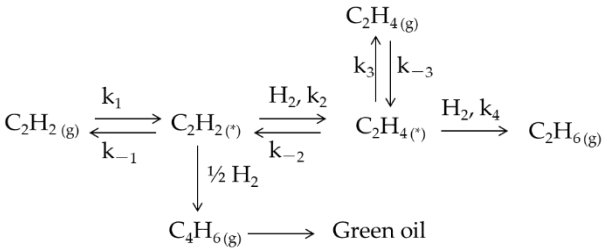

Scheme 1. Plausible reaction route for acetylene hydrogenation. The asterisk (*) represents the adsorbed state of the species on the catalyst surface.

The noble metal Pd is widely used in selective hydrogenation of acetylene and other auxiliary metals such as Ag, Cu, Au, and Zn are usually added to change the geometric and electronic effects of Pd, which allows regulating the adsorption of reactants and products on Pd and achieve a good catalytic effect [10,11]. Unfortunately, in the calcium carbide acetylene hydrogenation reaction, the acetylene concentration is so high that a high number of active sites are required, concomitantly increasing the catalyst cost. Therefore, the development of a cost-effective catalyst suitable for this reaction system with satisfactory activity is highly desirable. Among the nonprecious metals, Ni is considered the most active in the hydrogenation reaction, reaching a high acetylene conversion, albeit with a poor ethylene selectivity [12,13]. Compared with hydrogen, Ni has a stronger adsorption for acetylene, which facilitates the polymerization of acetylene to form green oil once it is adsorbed on the Ni surface [13]. Therefore, to enhance ethylene selectivity on Ni-based catalysts, the adsorption of ethylene and acetylene should be reduced to avoid over-hydrogenation of ethylene and polymerization to form green oil, respectively. To achieve this, a second metal can be introduced to change the electron cloud density on the Ni surface, thus changing the adsorption energy of Ni for acetylene and ethylene. In this context, the addition of metals such as Zn, Ga, and Ag on Ni catalysts has been investigated. Spanjers et al. reported that Ni/Zn intermetallic compounds significantly reduce the adsorption of acetylene compared to their Ni monometallic counterpart, thereby reducing the formation of oligomeric species and increasing ethylene selectivity [13]. Wang et al. demonstrated that the ethylene selectivity of Ni/SiO_2 could be enhanced from 55% to 75–81% in Ni_5Ga/SiO_2 after adding Ga, due to the Ga-induced change in the geometric and electronic effects of Ni atoms inhibiting excessive hydrogenation and polymerization [14]. Chen et al. reported that inserting In into a Ni/SiO_2 catalyst geometrically isolated Ni atoms and caused electron transfer from In to Ni, which reduced ethylene adsorption and inhibited acetylene polymerization, thereby improving ethylene selectivity from 45% to 60% [15]. Pei et al. reported the introduction of Ag in the Ni/SiO_2 catalyst, and the interaction between Ni and Ag improved the performance of the catalyst [16]. In addition, Yang et al. demonstrated by density functional theory (DFT) calculations that the addition of Cu to a Ni catalyst can reduce the adsorption energy of acetylene and increase the catalytic activity [17]. Meanwhile, Liu et al. reported the preparation of a NiCu nanoalloy catalyst using a layered double hydroxide for the ethylene-rich acetylene removal reaction [18]. Compared with the Ni monometallic catalyst, although the acetylene conversion decreased from 100% to 85%, the ethylene selectivity increased from 22.1% to 70.2%, and the catalyst stability was also improved, but they did not consider the effect of Cu content on the catalytic performance, and also ignored the green oil selectivity.

To gain more insight into the influence of adding Cu to Ni catalysts for pure acetylene hydrogenation to ethylene, we herein examine the performance of $NiCu_x$ catalysts considering green oil selectivity. We prepared a series of catalysts with different Cu/Ni molar ratios by coimpregnation, and used amino-modified MCM-41 as a support to improve the dispersibility of metal particles. Characterization

techniques such as X-ray diffraction (XRD) and transmission electron microscopy (TEM) were used to analyze the geometric structure of the catalyst, and the interaction between Ni and Cu was confirmed by High resolution transmission electron microscope (HRTEM), H_2 temperature-programmed reduction (H_2-TPR), and X-ray photoelectron spectroscopy (XPS) characterization. In addition, we calculated using DFT the adsorption energy of the catalyst for acetylene and ethylene before and after the addition of Cu. Furthermore, the reason for the different stability of the catalysts was investigated by thermogravimetric analysis (TGA).

2. Experimental Sections

2.1. Materials

MCM-41 (surface area: 1124.0 m^2/g) was purchased from Nanjing Xianfeng Nano Material Technology Co., Ltd. (Nanjing, China). Nickel nitrate hexahydrate ($Ni(NO_3)_2{\cdot}6H_2O$) (AR, 98%) and copper nitrate trihydrate ($Cu(NO_3)_2{\cdot}3H_2O$) (AR, 99%) were purchased from Shanghai Macklin Biochemical Technology Co., Ltd. (Shanghai, China). 3-aminopropyltriethoxysilane (APTES) (AR, 98%) was purchased from Aladdin Industrial Co., Ltd. (Shanghai, China).

2.2. Catalyst Preparation

MCM-41 was subjected to the following treatment, which was reported in our previous work [19,20]: 120 mL of toluene was placed in a 250 mL three-necked flask, 2 g of MCM-41 was added under stirring, and then 4.5 mL of 3-aminopropyltriethoxysilane (APTES) was added dropwise under N_2 protection. After 12 h, it was suction filtered, washed with deionized water, and then dried at 100 °C.

A series of catalysts were prepared by coimpregnation method. A certain amount of Nickel nitrate and Cupric nitrate was dissolved in 30 mL of deionized water, and 2 g of MCM-41 was added under stirring, ultrasonically dispersed for 10 min, stirred for 24 h, and then evaporated to dryness at 70 °C obtained solid powder. The dried sample was calcined in a muffle furnace at a rate of 5 °C/min to 400 °C for 4 h, and then reduced in a tube furnace under 10 vol% H_2/Ar atmosphere at a rate of 5 °C/min to 500 °C for 4 h to obtain the $NiCu_x$/MCM-41 catalysts (x represents the molar ratio of Cu to Ni). In this study, the Ni load was fixed at 1 wt%, and the Cu content was adjusted to achieve the Cu/Ni molar ratio of 0.05–2. For comparison, 1%Ni/MCM-41 and 1%Cu/MCM-41 catalysts were prepared following the same method.

2.3. Catalyst Characterization

The X-ray diffraction (XRD) pattern was obtained by measuring the catalyst on the Bruker D8 Advance X-ray diffractometer (Billerica, MA, USA) with Cu-Kα irradiation (λ = 1.5406 Å) as an X-ray source. We heated 20 mg catalyst before reduction to 900 °C at a heating rate of 10 °C/min on the Quantachrome Instruments automated chemisorption analyzer (Boynton Beach, FL, USA) to obtain the temperature-programmed reduction (TPR) pattern. Transmission electron microscopy (TEM) images were obtained with a Tecnai F30 field emission transmission electron microscope (Hillsboro, OR, USA) operating at 300 KV at room temperature. The X-ray photoelectron spectroscopy (XPS) data of Ni in the catalyst were obtained on a Thermo Fisher Scientific ESCALAB 250Xi X-ray photoelectron spectroscopy analyzer (Waltham, MA, USA). A Thermo-ICAP 6300 plasma emission spectrometer (Bremen, Germany) was used to obtain the actual Ni content of the catalyst. Before the test, the 0.1 g catalyst was completely dissolved into a clarified solution with hydrofluoric acid and aqua regia, and then diluted to a 50 mL volumetric bottle. Thermogravimetric (TG) analysis was performed to analyze the carbon deposit on the catalyst. The catalysts were analyzed on a Netzsch synchronous thermal analyzer (Selb, Germany) from room temperature to 900 °C with a 10 °C/min heating rate.

2.4. Catalytic Performance Test

The pure acetylene hydrogenation to ethylene reaction was performed continuously on a fixed bed reactor under 0.1 MPa. The catalyst (0.1 g) was placed into the reactor (a stainless steel tube with a diameter of 10 mm) and heated to 150 °C in H_2 (80 mL/min) to provide the initial temperature for the reaction. After the temperature was stabilized, the H_2 flow rate was adjusted to a certain value, a certain amount of acetylene was introduced into the reaction system, and the temperature was maintained at the specified reaction temperature (no other gas participates in the reaction). The raw materials, acetylene and hydrogen, were of more than 99.99 vol% purity. The gaseous products were analyzed online using a Shimadzu GC-2014C gas chromatograph (Shimadzu, Kyoto, Japan) and detected by a thermal conductivity detector.

Acetylene conversion (X) and product selectivity (S) were calculated using the following formulas:

$$X_{C_2H_2} = \frac{n_{C_2H_2(\text{inlet})} - n_{C_2H_2(\text{outlet})}}{n_{C_2H_2(\text{inlet})}}$$

$$S_{C_2H_4} = \frac{n_{C_2H_4(\text{outlet})}}{n_{C_2H_2(\text{inlet})} - n_{C_2H_2(\text{outlet})}}$$

$$S_{C_2H_6} = \frac{n_{C_2H_6(\text{outlet})}}{n_{C_2H_2(\text{inlet})} - n_{C_2H_2(\text{outlet})}}$$

$$S_{green\ oil} = 1 - S_{C_2H_4} - S_{C_2H_6}$$

In the above formula, green oil consists of C_{4+} hydrocarbons and carbon deposition based on carbon balance calculation.

Average turnover frequency (*TOF*) is an important parameter to evaluate the activity of catalyst, which was calculated as follows.

$$TOF_{C_2H_2} = \frac{X \times n_{C_2H_2}}{n_{(\text{Ni+Cu})} \times D}$$

X = the acetylene conversion, $n_{C_2H_2}$ = the molar rate of acetylene per second, $n_{(\text{Ni+Cu})}$ = the mole of Ni and Cu in the catalyst, D = dispersion calculated by particle size.

The stability test was conducted using fresh catalysts for continuous reaction until the catalyst is deactivated under optimal reaction conditions of 250 °C, 8000 mL·g^{-1}·h^{-1} and V(H_2)/V(C_2H_2) = 3. The catalyst testing process is consistent with the catalyst performance test process described above.

3. Results and Discussion

3.1. Catalyst Activity and Characterization

To determine the actual metal content in the catalyst and the molar ratio of Cu to Ni, we subjected the reduced catalyst to inductive coupled plasma (ICP) characterization. The results are shown in Table 1. The actual loading of Ni is close to the theoretical value, indicating that Ni was successfully loaded onto MCM-41. In contrast, the actual Cu loading was lower than the theoretical value, indicating that Cu was harder to load onto the support than Ni. As a result, the actual molar ratio of Cu to Ni was slightly lower than the theoretical value. Figure S1 shows the XRD patterns of catalysts after reduction at 500 °C. All samples had a broad and distinct peak between 20° and 40°, which can be assigned to the characteristic peak of SiO_2 in the MCM-41 support [21]. However, no characteristic peaks of Ni or Cu were observed in the samples, which might be due to the small size of the metal nanoparticles or to low metal loading [16].

Table 1. Metal loadings and Cu to Ni molar ratios of the $NiCu_x$/MCM-41 catalysts and other parameter.

Catalyst	Theoretical Loading (wt%)		Actual Loading [a] (wt%)		Actual Cu:Ni Molar Ratio	Dispersion [b]
	Ni	Cu	Ni	Cu		
Ni/MCM-41	1	/	1.12	/	/	0.25
$NiCu_{0.05}$/MCM-41	1	0.05	1.13	0.04	0.034	/
$NiCu_{0.125}$/MCM-41	1	0.13	1.18	0.11	0.085	0.20
$NiCu_{0.25}$/MCM-41	1	0.27	1.16	0.21	0.166	/
$NiCu_{0.5}$/MCM-41	1	0.54	1.04	0.38	0.337	0.21
$NiCu_1$/MCM-41	1	1.07	0.97	0.80	0.739	/
$NiCu_2$/MCM-41	1	2.12	1.06	1.61	1.398	/
Cu/MCM-41	/	1.0	/	0.71	/	/

[a] Obtained by ICP; [b] Obtained by TEM.

We characterized the particle size of the $NiCu_x$/MCM-41 (X = 0, 0.125, 0.5) catalysts by TEM (Figure 1). The metal particles are more uniformly dispersed on the MCM-41 surface, and the average particles of the Ni/MCM-41, $NiCu_{0.125}$/MCM-41, and $NiCu_{0.5}$/MCM-41 catalysts after reduction were calculated to be 3.99, 4.94, and 4.85 nm, respectively. Compared with the Ni/MCM-41 catalyst, the growth of the catalyst particles after Cu addition is small, but the metal particle size is still uniformly, and no larger particles or agglomeration appear. These results are consistent with the XRD results.

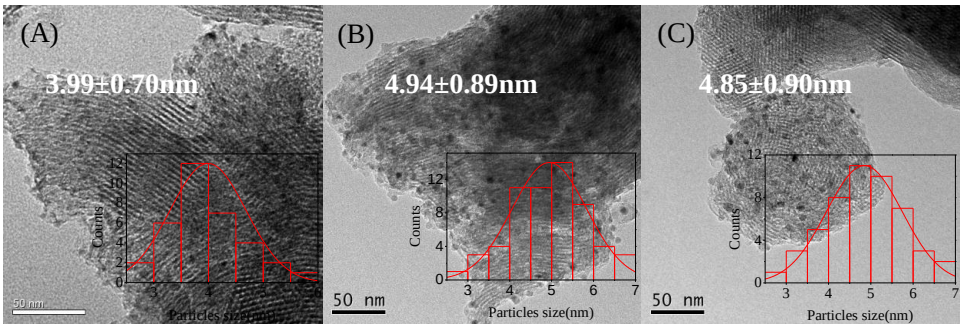

Figure 1. TEM images of (**A**) 1%Ni/MCM-41, (**B**) $NiCu_{0.125}$/MCM-41, and (**C**) $NiCu_{0.5}$/MCM-41.

We explored the effect of having different Cu/Ni molar ratio on the catalyst activity. The results are shown in Figure 2. Under the same reaction conditions, the acetylene conversion for the Ni/MCM-41 catalyst remained 100% within 9 h. The selectivity of ethylene, ethane, and green oil were 45%, 10%, and 45%, respectively. For the $NiCu_x$/MCM-41catalyst, with the increase of Cu content, the initial acetylene conversion in all cases reached 100%, but the stability gradually decreased, with the catalyst having the molar ratio Cu/Ni ≤ 0.25, being relatively stable during the test time. The ethylene selectivity first increased and then decreased, and the catalyst with Cu/Ni = 0.125 reached the optimal level. The ethane selectivity remained below 3%, and the green oil selectivity decreased first and then increased. This phenomenon is consistent with previous findings [15]. Finally, $NiCu_{0.125}$/MCM-41 exhibited the best hydrogenation activity. During the test period, the acetylene conversion remained 100%, the ethylene selectivity was 63%, the ethane selectivity was only approximately 2%, and the green oil selectivity was approximately 35%. Compared with the ethylene selectivity of the Ni/MCM-41 catalyst, that of the $NiCu_{0.125}$/MCM-41 catalyst increased by 18%, mainly because the addition of Cu reduced the formation of ethane and green oil. It is worth noting that the catalyst stability was negatively correlated with the green oil selectivity; the catalyst deactivated faster as the green oil selectivity increased, which indicates that the accumulation of green oil with reaction time was detrimental to the stability of catalyst. The TOF value of Ni/MCM-41, $NiCu_{0.125}$/MCM-41, and $NiCu_{0.5}$/MCM-41 catalysts were calculated as 1.87, 2.04 and 1.79, respectively (Figure 3). Obviously, compared with the other

two catalysts, $NiCu_{0.125}$/MCM-41 had the largest TOF value, indicating that the catalyst had excellent catalytic activity.

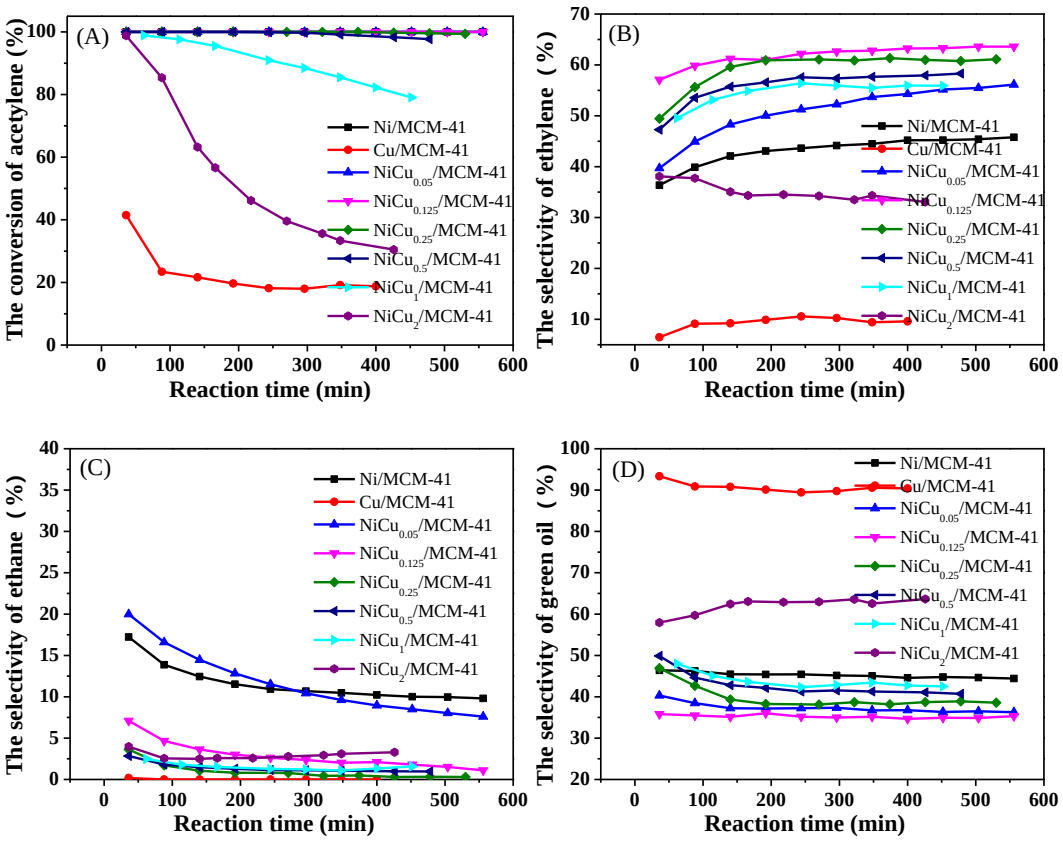

Figure 2. Catalytic performance of different catalysts at 8000 $mL \cdot g^{-1} \cdot h^{-1}$, 250 °C, and $V(H_2)/V(C_2H_2)$ = 3; (**A**) acetylene conversion, (**B**) ethylene selectivity, (**C**) ethane selectivity, (**D**) green oil selectivity.

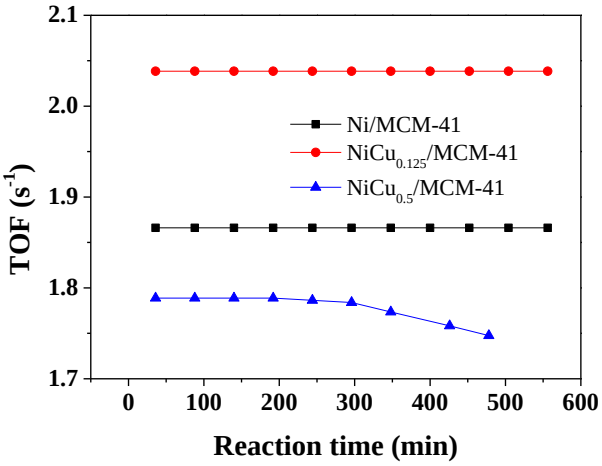

Figure 3. TOF value for the Ni/MCM-41, $NiCu_{0.125}$/MCM-41 and $NiCu_{0.5}$/MCM-41catalysts at 8000 $mL \cdot g^{-1} \cdot h^{-1}$, 250 °C, and $V(H_2)/V(C_2H_2)$ = 3.

To further understand the geometric structure of Ni–Cu in bimetallic catalysts, the lattice sizes of metal particles in the $NiCu_{0.125}$/MCM-41 and $NiCu_{0.5}$/MCM-41 catalysts were characterized by HRTEM (Figure 4). It was found that the lattice fringe of individual particles in the $NiCu_{0.125}$/MCM-41 and $NiCu_{0.5}$/MCM-41 catalysts was 0.206 and 0.207 nm, respectively, both between those of Ni[111]

(0.203 nm) and Cu[111] (0.209 nm), indicating that an intermetallic compound was formed between Ni and Cu [14,21].

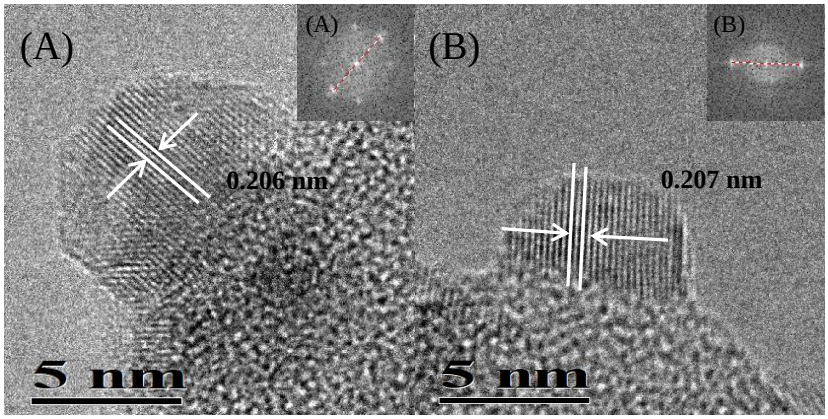

Figure 4. HRTEM image of (**A**) $NiCu_{0.125}$/MCM-41, (**B**) $NiCu_{0.5}$/MCM-41, the image inset in (**A**) and (**B**) are the corresponding Fast Fourier Transform (FFT) patterns.

Figure 5A shows the H_2-TPR curves of Ni/MCM-41 and Cu/MCM-41 and the bimetallic $NiCu_x$/MCM-41 catalysts. Ni/MCM-41 showed a wide peak at 380–630 °C, which is attributed to the reduction of NiO particles having strong interactions with the MCM-41 support [22,23]. Meanwhile, Cu/MCM-41 exhibited two distinct peaks at 227 °C and 310 °C due to the reduction of Cu^{2+} and Cu^{1+}, respectively [24,25]. The series of Ni–Cu/MCM-41 catalysts displayed two main reduction peaks, a low temperature reduction peak attributed to the reduction of copper oxide and a high temperature reduction peak that can be assigned to the reduction of nickel oxide. The shift of the reduction peak to low temperature indicates the occurrence of an interaction between Ni and Cu. As the Cu content increased, both reduction peaks shifted toward the low temperature direction; the decrease in the reduction temperature of nickel oxide is attributed to the fact that Cu species participate in the reduction of Ni species [26,27]. Moreover, as the Cu content increased, the reduction peak of nickel oxide became wider, further indicating that there was a strong interaction between Ni and Cu species, which led to the formation of a Ni–Cu intermetallic compound [15]. This result is consistent with the HRTEM result.

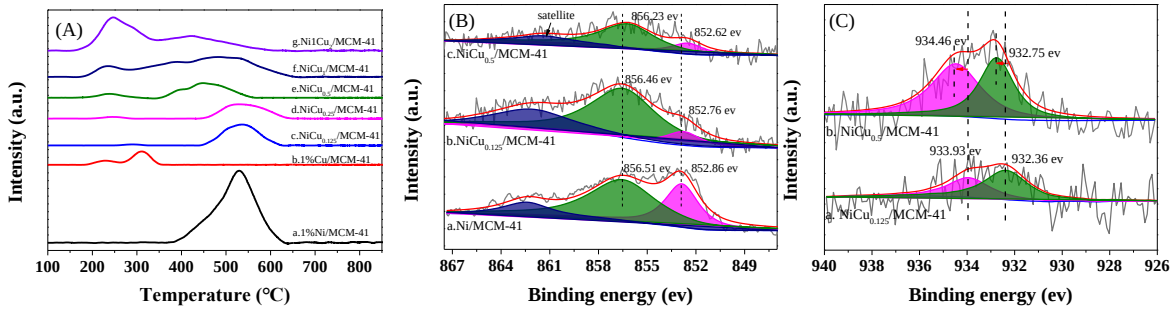

Figure 5. (**A**) H_2-TPR profiles of the catalysts. (**B**) $Ni2p_{3/2}$ XPS spectra of the catalysts. (**C**) $Cu2p_{3/2}$ XPS spectra of the catalysts.

Figure 5B display the XPS spectra in the $Ni2p_{3/2}$ region for Ni/MCM-41, $NiCu_{0.125}$/MCM-41, and $NiCu_{0.5}$/MCM-41. In the spectrum of Ni/MCM-41, the electron binding energy at 852.86 eV corresponds to zero-valent metal nickel, and the binding energy at 856.51 eV and 862.41 eV can be assigned to nickel oxide with the $Ni2p_{3/2}$ and its satellite peak, respectively [28–30]. After the addition of the Cu species, $Ni2p_{3/2}$ shifted to a low binding energy of 852.76 eV for $NiCu_{0.125}$/MCM-41 and 852.62 eV for $NiCu_{0.5}$/MCM-41. Figure 5C display the XPS spectra in the $Cu2p_{3/2}$ region for $NiCu_{0.125}$/MCM-41, and $NiCu_{0.5}$/MCM-41. The low electron binding energy and high electron binding energy are attributed to

Cu^0 and Cu^{2+}, respectively [18] and $Cu2p_{3/2}$ shifts to a high binding energy with the increase of Cu content. These changes in the binding energies of Ni and Cu indicate that the electron transfer from Cu to Ni changed the electron cloud density of the Ni surface, and is consistent with the formation of a Ni–Cu intermetallic compound [27,31]. This result is in agreement with those of the HRTEM and TPR analysis.

Moreover, the adsorption energy of acetylene, ethylene, and hydrogen on the metal clusters was determined by DFT calculation. All simulations were performed using the Guassian09 software package (Gaussian Inc.: Wallingford, CT, USA) [32] with the hybrid B3LYP density functional method [33]. The 6-31G basis set was applied for nonmetals and the LANL2DZ pseudopotential basis set for metals. According to the approximate actual molar ratio of Cu to Ni obtained from the experimental results, we constructed Ni–Cu metal clusters as the initial model for the evaluation of the adsorption. The model depicted in Figure S2 showed the most stable optimized structure for each catalyst. After that, we studied the adsorption of acetylene and ethylene molecules by five different catalysts, and obtained the optimal adsorption configuration. The optimized adsorption structure can be seen in Figure S3, and the adsorption energy is shown in Figure 6. From the comparison of the adsorption energy, it can be extracted that the acetylene adsorption energy was higher than the hydrogen adsorption energy for all the catalysts, which indicates that acetylene was more easily adsorbed at the active site during the adsorption process. Although the adsorption of acetylene on Ni clusters was significantly reduced after the addition of Cu, there was no significant difference in the adsorption energy of acetylene for the metal clusters with different molar ratios of Cu to Ni. In any case, the decrease in the acetylene adsorption energy reduces the formation of polymer. In addition, the hydrogen adsorption on $NiCu_x$ metal clusters was lower than that on Ni metal clusters, which was advantageous for reducing excessive hydrogenation of ethylene. At the same time, the addition of Cu also reduced the adsorption of ethylene, which accelerated the desorption of ethylene product from the active site, resulting in higher ethylene selectivity. Interestingly, the adsorption energy of metal clusters to ethylene decreased with the decrease of Cu content, which is consistent with the experimental results that indicate that the ethylene selectivity increases with the decrease of Cu content in the catalyst. Overall, the formation of Ni–Cu intermetallic compounds changes the adsorption of Ni to acetylene, ethylene, and hydrogen, thus improving the ethylene selectivity.

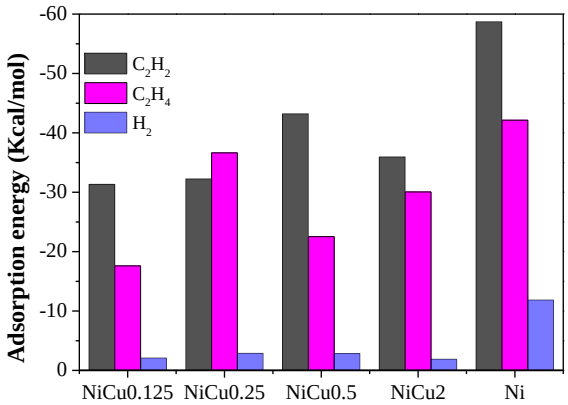

Figure 6. Adsorption energy of C_2H_2 and C_2H_4 on the different catalysts.

To clarify the reason for the different stability of the catalysts having different Cu/Ni molar ratios, we conducted thermogravimetric tests on the catalysts after reaction for 9 h. The results are shown in Figure 7. Two significant weightlessness peaks appeared for all catalysts. The weightlessness at low temperature (210–390 °C) can be attributed to the combustion of light hydrocarbons adsorbed in the catalyst pores or on the catalyst surface [34,35], whereas the weightlessness at high temperature (>390 °C) is attributable to the combustion of heavy hydrocarbons or coke deposited on the catalyst surface [36,37]. Note that compared with the Ni catalyst, the weightlessness peak significantly moved

toward the high temperature region after adding Cu, which indicates that the green oil deposits changed to hydrocarbons heavier than those deposited on the Ni catalyst surface. As can be seen from Figure 7, except $NiCu_{0.125}$/MCM-41, the mass loss was lower than that of the Ni catalyst and increased with the Cu content. This indicates that the addition of an appropriate amount of Cu reduced carbon deposition, whereas the excess amount of Cu had the opposite effect, leading to catalyst deactivation as the Cu content increased. Interestingly, the weight loss of different Cu/Ni molar ratios after the reaction can be positively correlated with the selectivity of green oil in the reaction, indicating that the carbon deposition was mainly caused by green oil.

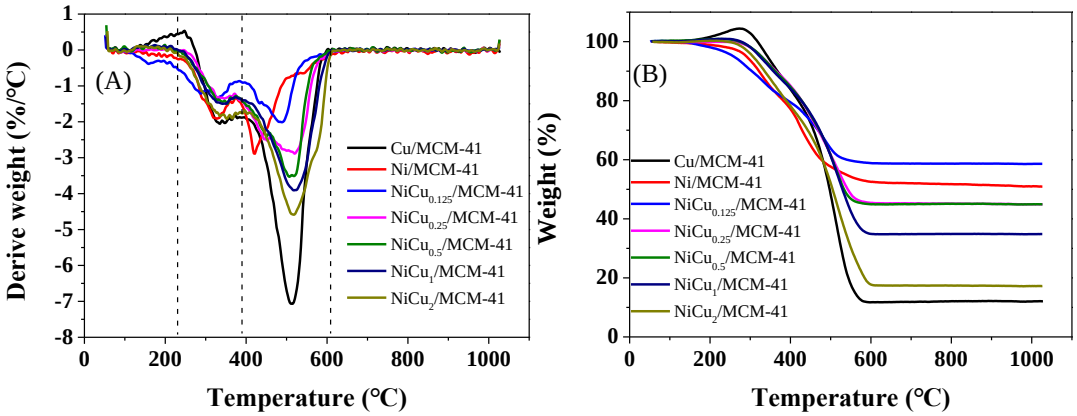

Figure 7. DTG (**A**) and TG (**B**) curves of catalysts after reaction.

3.2. Optimization of Reaction Conditions

Considering the above study, which evinced the good stability and optimal selectivity of $NiCu_{0.125}$/MCM-41, this catalyst was selected to explore the effects of the reaction conditions (i.e., temperature, acetylene space velocity, acetylene to hydrogen ratio) on the conversion and product selectivity. Figure S4A,B show the effect of reaction temperature on acetylene conversion and ethylene selectivity. The acetylene conversion was almost above 97% in the 150–300 °C temperature range. The catalyst stability increased significantly with temperature (150–250 °C), which may be due to volatilization of part of the hydrocarbons attached to the catalyst surface at high temperature. However, at 300 °C, the stability of the catalyst decreased slightly, most likely due to catalyst sintering. By contrast, the effect of temperature on ethylene selectivity was negligible.

The effect of acetylene space velocity on acetylene conversion and ethylene selectivity is evaluated in Figure S4C,D, which show that the catalyst stability decreased gradually with the increase of acetylene space velocity, and the ethylene selectivity increased significantly first and then remained basically unchanged. This is mainly caused by the increase in the accumulation of green oil on the catalyst surface at high space velocity, whereas the over-hydrogenation of ethylene into ethane is hampered at short residence times [38,39]. Figure S4E,F show the effect of the acetylene to hydrogen ratio on acetylene conversion and ethylene selectivity. For hydrogen to acetylene ratios in the range of 2–6, the acetylene conversion was above 98% and relatively stable as the ratio increased; the ethylene selectivity increased first and then remained virtually unaltered. This result is consistent with the literature report [40], and is due to the competitive adsorption of acetylene, hydrogen, and ethylene on the catalyst in this reaction. With the increase of the hydrogen to acetylene ratio from 2 to 3, the hydrogen coverage on the catalyst surface was enhanced, which weakened the adsorption of acetylene, reduced the probability of acetylene polymerization, and increased ethylene selectivity. At higher hydrogen concentrations (hydrogen to acetylene ratio > 3), the hydrogen adsorbed at the active site caused further hydrogenation of the intermediate ethylene to ethane [9,39]. Finally, the optimal reaction conditions were T = 250 °C, GHSV = 8000 $mL \cdot g^{-1} \cdot h^{-1}$, and hydrogen to acetylene ratio = 3. In these

conditions, the acetylene conversion could be kept at 100% within 9 h, and the ethylene selectivity reached 63.6%.

3.3. Stability Test

To investigate the effect of Cu on catalysts stability, stability tests were conducted for $NiCu_{0.125}$/MCM-41 and Ni/MCM-41. It can be seen from the experimental results depicted in Figure 8 that the stability improved significantly after adding Cu and the TOF value of $NiCu_{0.125}$/MCM-41 higher than that of Ni/MCM-41. The acetylene conversion of $NiCu_{0.125}$/MCM-41 maintains over 99% for 42 h, whereas the same value of acetylene conversion was kept for 24 h for the Ni/MCM-41 catalyst. According to the TG result displayed in Figure 7B, the weight loss of $NiCu_{0.125}$/MCM-41 was lower than that of Ni/MCM-41 after the reaction, indicating that the decrease of carbon deposition on the catalyst surface was the reason for the good stability of the $NiCu_{0.125}$/MCM-41 catalyst.

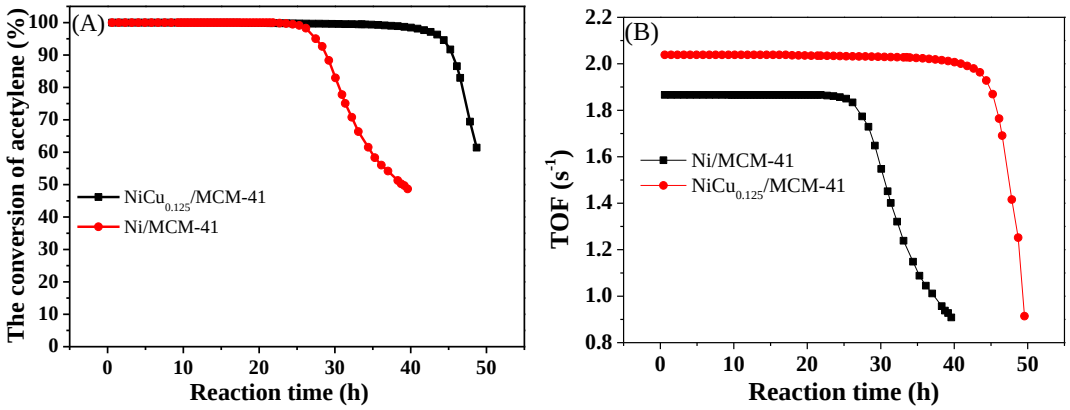

Figure 8. Catalytic stability (**A**) and the average turnover frequency (**B**) of the Ni/MCM-41 and $NiCu_{0.125}$/MCM-41 catalysts at 250 °C and 8000 $mL \cdot g^{-1} \cdot h^{-1}$.

4. Conclusions

A series of Ni–Cu bimetallic catalysts supported by amino-modified MCM-41 were prepared by coimpregnation. Compared with the Ni/MCM-41 catalyst, the ethylene selectivity of the bimetallic $NiCu_x$/MCM-41 catalyst was significantly improved, mainly attribute to the interaction between Ni and Cu reducing the adsorption energy of acetylene and ethylene, thereby hindering acetylene polymerization and ethylene hydrogenation. In addition, with the decrease of Cu content, the stability of the catalyst gradually increased, which was mainly due to the decrease of carbon deposition. In general, the $NiCu_{0.125}$/MCM-41 catalyst exhibited better ethylene selectivity and stability than the Ni/MCM-41 catalyst. Our results provide useful information for the design of Ni-based catalysts for the selective hydrogenation of pure acetylene to ethylene.

Supplementary Materials: The following are available online at http://www.mdpi.com/2079-4991/10/3/509/s1, Figure S1: XRD patterns of the catalysts, Figure S2: Optimal structure of the catalysts, Figure S3: Adsorption configuration of C_2H_2, C_2H_4, and H_2 on several catalysts, Figure S4: Effect of reaction temperature on (A) acetylene conversion and (B) ethylene selectivity at 8000 $mL \cdot mg^{-1} \cdot h^{-1}$ and $V(H_2)/V(C_2H_2) = 3$. Effect of acetylene space velocity on (C) acetylene conversion and (D) ethylene selectivity at 250 °C and $V(H_2)/V(C_2H_2) = 3$. Effect of acetylene to hydrogen ratio on (E) acetylene conversion and (F) ethylene selectivity at 250 °C and 8000 $mL \cdot mg^{-1} \cdot h^{-1}$.

Author Contributions: Performed experiments and analyzed data, S.Z. and Z.X.; proposed and planned the research, L.K.; Established adsorption model and calculated, X.Z.; Supervised the experiments and acquired funding, M.Z. All authors have read and agreed to the published version of the manuscript.

Funding: This research was funded by the International Corporation of S&T Project in Xinjiang Bingtuan (2018BC003) and the International Corporation of S&T Project in Shihezi University (GJHZ201701).

Conflicts of Interest: The authors declare no conflict of interest.

References

1. Rahimpour, M.R.; Dehghani, O.; Gholipour, M.R.; Shokrollahi Yancheshmeh, M.S.; Seifzadeh Haghighi, S.; Shariati, A. A novel configuration for Pd/Ag/α-Al_2O_3 catalyst regeneration in the acetylene hydrogenation reactor of a multi feed cracker. *Chem. Eng. J.* **2012**, *198*, 491–502. [CrossRef]
2. Zhang, L.; Ding, Y.; Wu, K.H.; Niu, Y.; Luo, Y.; Yang, X.; Zhang, B.; Su, D. Pd@C core-shell nanoparticles on carbon nanotube as highly stable and selective catalysts for hydrogenation of acetylene to ethylene. *Nanoscale* **2017**, *9*, 14317–14321. [CrossRef] [PubMed]
3. Tysoe, W.T.; Nyberg, G.L.; Lambert, R.M. Low temperature catalytic chemistry of the Pd(111) surface: Benzene and ethylene from acetylene. *J. Chem. Soc. Chem. Commun.* **1983**, 623–625. [CrossRef]
4. Mccue, A.J.; Shepherd, A.M.; Anderson, J.A. Optimisation of preparation method for Pd doped Cu/Al_2O_3 catalysts for selective acetylene hydrogenation. *Catal. Sci. Technol.* **2015**, *5*, 2880–2890. [CrossRef]
5. Cao, X.; Mirjalili, A.; Wheeler, J.; Wheeler, J.; Xie, W.; Jang, B. Investigation of the preparation methodologies of Pd-Cu single atom alloy catalysts for selective hydrogenation of acetylene. *Front. Chem. Sci. Eng.* **2015**, *9*, 442–449. [CrossRef]
6. Borodziński, A.; Bond, G.C. Selective Hydrogenation of Ethyne in Ethene Inich Streams on Palladium Catalysts, Part 2: Steady logtate Kinetics and Effects of Palladium Particle Size, Carbon Monoxide, and Promoters. *Catal. Rev.* **2008**, *50*, 379–469. [CrossRef]
7. Trimm, D.L.; Liu, I.O.Y.; Cant, N.W. The oligomerization of acetylene in hydrogen over Ni/SiO_2 catalysts: Product distribution and pathways. *J. Mol. Catal. A Chem.* **2008**, *288*, 63–74. [CrossRef]
8. Molnár, Á.; Sárkány, A.; Varga, M. Hydrogenation of Carbon-Carbon Multiple Bonds: Chemo-, Regio- and Stereo-Selectivity. *J. Mol. Catal. A Chem.* **2001**, *173*, 185–221. [CrossRef]
9. Ahn, I.Y.; Lee, J.H.; Kum, S.S.; Moon, S.H. Formation of C4 species in the deactivation of a Pd/SiO_2 catalyst during the selective hydrogenation of acetylene. *Catal. Today* **2007**, *123*, 151–157. [CrossRef]
10. Chesnokov, V.V.; Chichkan, A.S.; Ismagilov, Z.R. Properties of Pd-Ag/C catalysts in the reaction of selective hydrogenation of acetylene. *Kinet. Catal.* **2017**, *58*, 649–654. [CrossRef]
11. Pongthawornsakun, B.; Mekasuwandumrong, O.; Santos Aires, F.J.C.; Büchel, B.; Baiker, A.; Pratsinis, S.E.; Panpranot, J. Variability of particle configurations achievable by 2-nozzle flame syntheses of the Au-Pd-TiO_2, system and their catalytic behaviors in the selective hydrogenation of acetylene. *Appl. Catal. A Gen.* **2018**, *549*, 1–7. [CrossRef]
12. Studt, F.; Abild-Pedersen, F.; Bligaard, T.; Sørensen, R.Z.; Christensen, C.H.; Nørskov, J.K. Identification of Non-Precious Metal Alloy Catalysts for Selective Hydrogenation of Acetylene. *Science* **2008**, *320*, 1320–1322. [CrossRef] [PubMed]
13. Spanjers, C.S.; Held, J.T.; Jones, M.J.; Stanley, D.D.; Sim, R.S.; Janik, M.J.; Rioux, R.M. Zinc inclusion to heterogeneous nickel catalysts reduces oligomerization during the semi-hydrogenation of acetylene. *J. Catal.* **2014**, *316*, 164–173. [CrossRef]
14. Wang, L.; Li, F.; Chen, Y.; Chen, J. Selective hydrogenation of acetylene on SiO_2 -supported Ni-Ga alloy and intermetallic compound. *J. Energy Chem.* **2019**, *29*, 40–49. [CrossRef]
15. Chen, Y.; Chen, J. Selective hydrogenation of acetylene on SiO_2 supported Ni-In bimetallic catalysts: Promotional effect of In. *Appl. Surf. Sci.* **2016**, *387*, 16–27. [CrossRef]
16. Pei, G.X.; Liu, X.Y.; Wang, A.; Su, Y.; Li, L.; Zhang, T. Selective hydrogenation of acetylene in an ethylene-rich stream over silica supported Ag-Ni bimetallic catalysts. *Appl. Catal. A Gen.* **2017**, *545*, 90–96. [CrossRef]
17. Yang, B.; Burch, R.; Hardacre, C.; Headdock, G.; Hu, P. Origin of the Increase of Activity and Selectivity of Nickel Doped by Au, Ag, and Cu for Acetylene Hydrogenation. *ACS Catal.* **2012**, *2*, 1027–1032. [CrossRef]
18. Liu, Y.; Zhao, J.; Feng, J.; He, Y.; Du, Y.; Li, D. Layered double hydroxide-derived Ni-Cu nanoalloy catalysts for semi-hydrogenation of alkynes: Improvement of selectivity and anti-coking ability via alloying of Ni and Cu. *J. Catal.* **2018**, *359*, 251–260. [CrossRef]
19. Dai, B.; Wen, B.; Zhu, M.; Kang, L.; Yu, F. Nickel catalysts supported on amino-functionalized MCM–41 for syngas methanation. *RSC Adv.* **2016**, *6*, 66957–66962. [CrossRef]
20. Luo, G.; Kang, L.; Zhu, M.; Dai, B. Highly active phosphotungstic acid immobilized on amino functionalized MCM-41 for the oxidesulfurization of dibenzothiophene. *Fuel Process. Technol.* **2014**, *118*, 20–27. [CrossRef]
21. Chai, M.; Liu, X.; Li, L.; Pei, G.; Ren, Y.; Su, Y.; Cheng, H.; Wang, A.; Zhang, T. SiO_2 -supported Au-Ni bimetallic catalyst for the selective hydrogenation of acetylene. *Chin. J. Catal.* **2017**, *38*, 1338–1346. [CrossRef]

22. Bayraktar, O.; Kugler, E.L. Temperature-programmed reduction of metal-contaminated fluid catalytic cracking (FCC) catalysts. *Appl. Catal. A Gen.* **2004**, *260*, 125–132. [CrossRef]
23. Nima, B.; Mehran, R.; Fereshteh, M. Methane dissociation to CO_x-free hydrogen and carbon nanofiber over Ni-Cu/Al_2O_3 catalysts. *Fuel* **2017**, *195*, 8–96.
24. Wang, X.; Zhu, M.; Dai, B. Effect of Phosphorus Ligand on Cu-based Catalysts for Acetylene Hydrochlorination. *ACS Sustain. Chem. Eng.* **2019**, *7*, 6170–6177. [CrossRef]
25. Balaraju, M.; Rekha, V.; Prasad, P.S.S.; Prasad, R.B.N.; Lingaiah, N. Selective Hydrogenolysis of Glycerol to 1, 2 Propanediol Over Cu–ZnO Catalysts. *Catal. Lett.* **2008**, *126*, 119–124. [CrossRef]
26. Naresh, G.; Velisoju, V.K.; Chatla, A.; Venu, B.; Tardio, J.; Patel, J.; Akula, V. Promotional effect of Cu and influence of surface Ni-Cu alloy for enhanced H_2 yields from CH_4 decomposition over Cu modified Ni supported on MCM-41 catalyst. *Energy Fuels* **2018**, *32*, 4008–4015.
27. Yang, Z.; Liu, Y.; Liu, D.; Meng, X.; Liu, C. Hydroisomerization of, n -octane over bimetallic Ni-Cu/SAPO-11 catalysts. *Appl. Catal. A Gen.* **2017**, *543*, 274–282. [CrossRef]
28. Liu, Z.D.; Yin, Z.Y.; Du, Z.H.; Yang, Y.; Zhu, M.M.; Xie, L.H.; Huang, W. Low temperature growth of graphene on Cu-Ni alloy nanofibers for stable, flexible electrodes. *Nanoscale* **2014**, *6*, 5110–5115. [CrossRef]
29. Khromova, S.A.; Smirnov, A.A.; Bulavchenko, O.A.; Saraev, A.A.; Kaichev, V.V.; Reshetnikov, S.I.; Yakovlev, V.A. Anisole hydrodeoxygenation over Ni-Cu bimetallic catalysts: The effect of Ni/Cu ratio on selectivity. *Appl. Catal. A Gen.* **2014**, *470*, 261–270. [CrossRef]
30. Zhang, M.J.; Li, P.P.; Zhu, M.Y.; Tian, Z.Q.; Dan, J.M.; Li, J.B.; Dai, B.; Yu, F. Ultralow-weight loading Ni catalyst supported on two-dimensional vermiculite for carbon monoxide methanation. *Chin. J. Chem. Eng.* **2018**, *26*, 107–112. [CrossRef]
31. Hsieh, H.H.; Chang, Y.K.; Pong, W.F.; Pieh, J.Y.; Tseng, P.K.; Sham, T.K.; Coulthard, I.; Naftel, S.J.; Lee, J.F.; Chung, S.C.; et al. Electronic structure of Ni-Cu alloys: The d-electron charge distribution. *Phys. Rev. B* **1998**, *57*, 15204–15210. [CrossRef]
32. Frisch, M.J.; Trucks, G.W.; Schlegel, H.B.; Scuseria, G.E.; Robb, M.A.; Cheeseman, J.R.; Scalmani, G.; Barone, V.; Mennucci, B.; Petersson, G.A.; et al. *Gaussian 09*; Gaussian, Inc.: Wallingford, CT, USA, 2009.
33. Lee, C.; Yang, W.; Parr, R.G. Development of the Colle-Salvetti correlation-energy formula into a functional of the electron density. *Phys. Rev. B* **1988**, *37*, 785–789. [CrossRef] [PubMed]
34. Kim, W.J.; Kang, J.H.; Ahn, I.Y.; Moon, S.H. Deactivation behavior of a TiO_2-added Pd catalyst in acetylene hydrogenation. *J. Catal.* **2004**, *226*, 226–229. [CrossRef]
35. Kim, W.J.; Moon, S.H. Modified Pd catalysts for the selective hydrogenation of acetylene. *Catal. Today* **2012**, *185*, 2–16. [CrossRef]
36. Ravanchi, M.T.; Sahebdelfar, S. Pd-Ag/Al_2O_3 Catalyst: Stages of Deactivation in Tail-End Acetylene Selective Hydrogenation. *Appl. Catal. A Gen.* **2016**, *525*, 197–203. [CrossRef]
37. Cao, Y.; Sui, Z.J.; Zhu, Y.; Zhou, X.; Chen, D. Selective Hydrogenation of Acetylene over Pd-In/Al_2O_3 Catalyst: Promotional Effect of Indium and Composition-dependent Performance. *ACS Catal.* **2017**, *226*, 226–229. [CrossRef]
38. Dong, M.; Pan, Z.; Peng, Y.; Meng, X.; Mu, X.; Zong, B.; Zhang, J. Selective acetylene hydrogenation over core–shell magnetic Pd-supported catalysts in a magnetically stabilized bed. *AIChE J.* **2008**, *54*, 1358–1364. [CrossRef]
39. Hou, R.; Wang, T.; Lan, X. Enhanced Selectivity in the Hydrogenation of Acetylene due to the Addition of a Liquid Phase as a Selective Solvent. *Ind. Eng. Chem. Res.* **2013**, *52*, 13305–13312. [CrossRef]
40. García-Mota, M.; Bridier, B.; Pérez-Ramírez, J.; López, N. Interplay between carbon monoxide, hydrides, and carbides in selective alkyne hydrogenation on palladium. *J. Catal.* **2010**, *273*, 92–102. [CrossRef]